ACADEMIC PRESS

Available online at www.sciencedirect.com

SCIENCE DIRECT®

Icarus 163 (2003) 135–141

ICARUS

www.elsevier.com/locate/icarus

Multispectral analysis of Asteroid 3 Juno taken with the 100-inch telescope at Mount Wilson Observatory

Sallie Baliunas,[a] Robert Donahue,[a] Michael R. Rampino,[b,c,*] Michael J. Gaffey,[d] J. Christopher Shelton,[e] and Subhanjoy Mohanty[f]

[a] *Harvard-Smithsonian Center for Astrophysics, Cambridge, MA 02138, USA*
[b] *Earth & Environmental Science Program, New York University, New York, NY 10003, USA*
[c] *NASA, Goddard Institute for Space Studies, New York, NY 10025, USA*
[d] *Department of Space Studies, University of North Dakota, 4149 Campus Road, Grand Forks, ND 58202-9008, USA*
[e] *Mount Wilson Institute, Pasadena, CA 91106, USA*
[f] *Department of Astronomy, University of California-Berkeley, Berkeley, CA 94720, USA*

Received 28 September 2001; revised 6 January 2003

Abstract

High-resolution multispectral images of main-belt asteroid 3 Juno were taken at visible and near-IR wavelengths with the 100-inch telescope at Mount Wilson Observatory equipped with an adaptive optics system. The images show spectral features that may represent a large relatively recent impact that deeply excavated the coarse-grained olivine–pyroxene-rich crust of the asteroid.

Introduction

3 Juno is an S(IV)-type main-belt asteroid with a diameter of ~240 km. The spectrum of Juno obtained previously with ground-based telescopes indicates the presence of an olivine–pyroxene mixture on its surface and 3 Juno was previously identified as one of the three most likely candidates for parent body of ordinary chondrite meteorites (Gaffey et al., 1993a). Here we utilize new ground-based high-resolution multispectral imaging of Juno to investigate the areal compositional variations and surface features of the asteroid.

Observations and data reduction

Juno was observed with the natural guide-star adaptive optics system (ADOPT) (Shelton et al., 1996, 1997) on the 100-in. Hooker telescope at Mount Wilson Observatory at wavelengths of 500, 700, 833, and 934 nm (Fig. 1). The Juno images were taken on 15 October 1996, near opposition. Resolution of the images is near the telescope's diffraction limit (80 mas at 833 nm), and the images were deconvolved with the Lucy–Richardson algorithm using 80 iterations. At the time of observation (1996 Oct. 15; 5:48–8:44 UT) (right ascension, 0 h 52 m; declination, −5°59′), Juno was 1.115 AU from the Earth and 2.091 AU from the Sun, at a solar phase angle of 7.8°. The asteroid's magnitude was 7.61, and the angular diameter of the asteroid was about 330 mas, based on an effective diameter of 267 km from occultation measurements (Millis et al., 1991). Juno was observed over a period of four hours centered on zenith crossing in order to minimize compensation for atmospheric dispersion.

Observations of a single, nearby star of similar *R*-magnitude to Juno (SAO 129094) were made in each filter at times before and after the Juno observations. A series of four images in each filter was taken of SAO129094. The star images were used to determine an average point-spread function (PSF), which was then applied by the Lucy–Ri-

* Corresponding author. Earth and Environmental Science Program, New York University, 100 Washington Square East Room 1009, New York, NY 10003. Fax: +1-212-995-4015.
E-mail address: michael.rampino@nyu.edu (M.R. Rampino).

0019-1035/03/$ – see front matter © 2003 Elsevier Science (USA). All rights reserved.
doi:10.1016/S0019-1035(03)00049-6

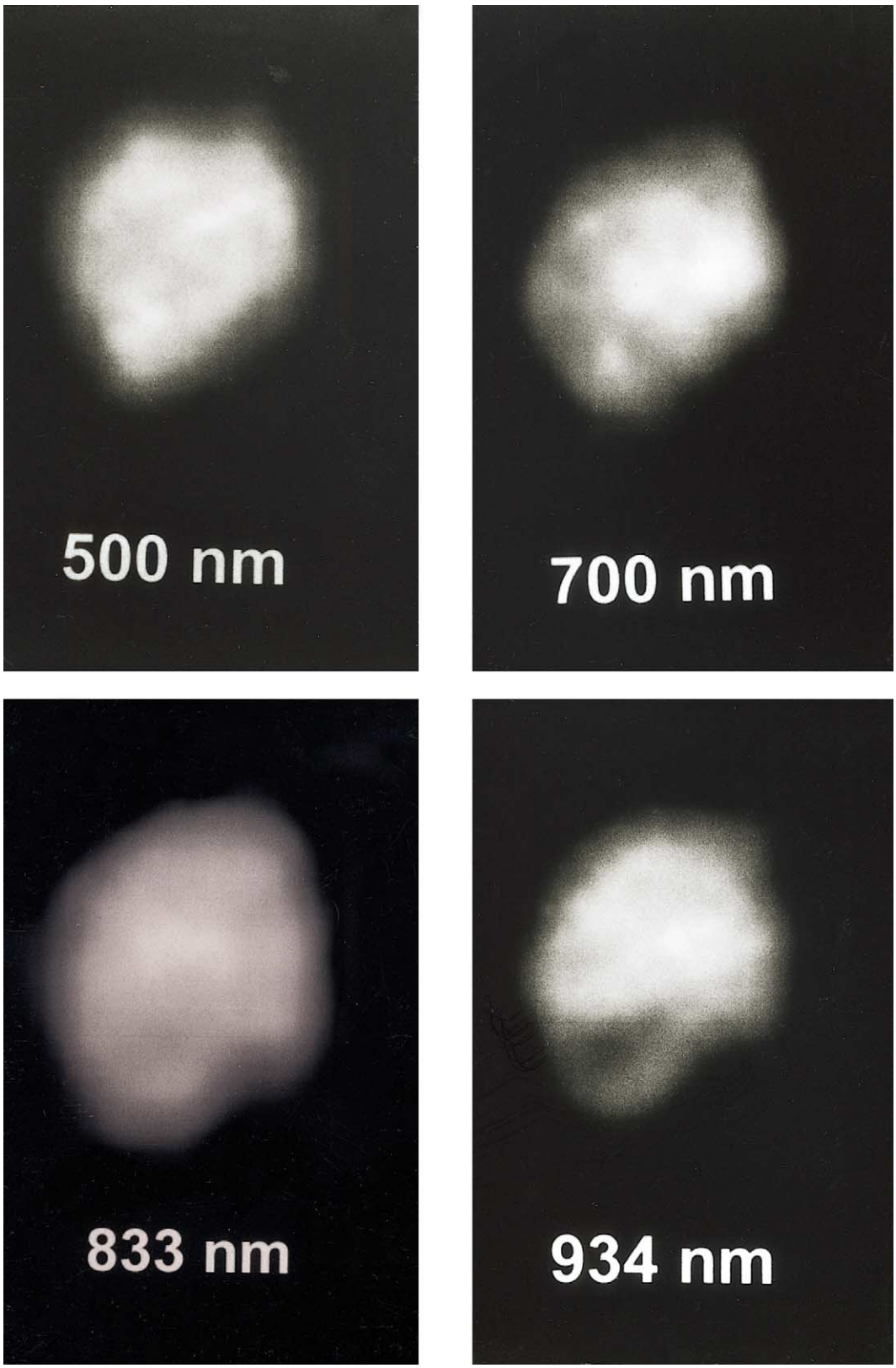

Fig. 1. Images of asteroid 3 Juno obtained with the 100-in. Hooker telescope at Mount Wilson Observatory on 15 October 1996, with Juno near opposition and illuminated at a solar phase angle of 7.8° (see text). Images have been processed by a deconvolution method described in the text. Images obtained at wavelengths of 500 nm, 700 nm, 833 nm, and 934 nm.

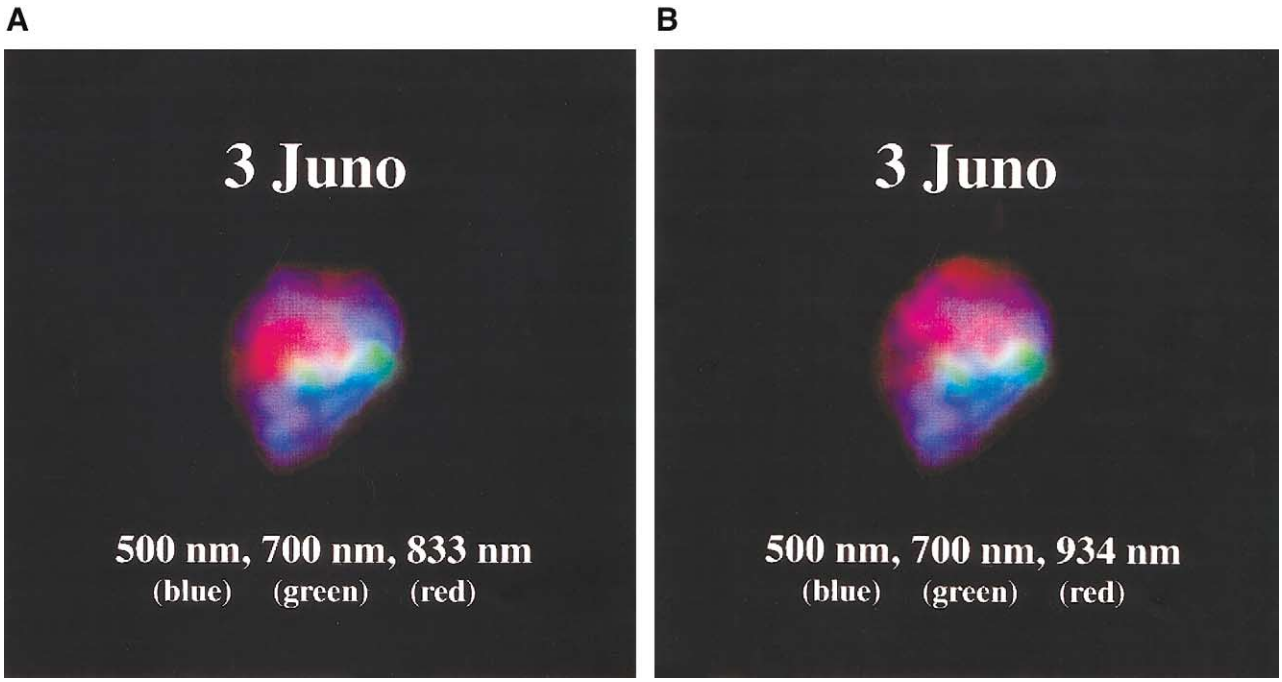

Fig. 2. Composite false-color multispectral images of asteroid 3 Juno produced by combining images from Fig. 1. (A) Images at 500, 700, and 833 nm were combined by assigning the brightest at each of those filters to the colors blue, green, and red, respectively. Higher albedo at different wavelengths corresponds to a stronger color or combination of colors. (B) The 833 nm image has been replaced with the 934 nm image (red). The bluer colors in the lower portion of the Juno images show the enhanced absorption at 934 nm.

chardson deconvolution calculation. As expected, the PSF for any filter varied (but only slightly) with time as atmospheric conditions changed. The maximum difference in the full-width at half-intensity of the point-spread function in the shortest wavelength filter (500 nm), which is the most demanding on system performance, was 2 pixels (i.e., the width varied from 6 to 8 pixels), or ~0.04″, over two hours. (The original PSF star images, raw Juno images, and processed images are available at http://cfa-www.harvard.edu/~donahue/Projects/Juno.)

Initial deconvolution showed that each Juno image is accompanied by a ghost, ~0.25″ (11 pixels) above the real Juno image. Such ghosts were a problem in the first year of operation of the ADOPT system, but with the refinement of alignment and operating procedures, they have been eliminated. We chose to compensate for the ghosts by adding an artificial ghost to each PSF image and deconvolving with this modified PSF. The artificial ghost was constructed from the original PSF by reducing the real PSF intensity by a factor of ~50% and shifting it 11 pixels above the original image. Deconvolution of this modified PSF largely removes the ghost from the results; however, a faint residual ghost can still be seen in the images.

A large circular feature is suggested in the lower left quadrant of the images, especially those at 0.833 and 0.943 μm. The images taken at 0.500 and 0.700 μm show relatively uniform brightness across the asteroid's surface (Fig. 1). By contrast, the image at 0.934 μm shows a strong decrease in brightness in the lower left quadrant. The 0.833 μm image shows a similar, but less pronounced, decrease in reflectance in the same region.

In order to clarify the areal relationships between reflectance and wavelength, composite false-color multispectral images (Fig. 2) were produced by combining the 0.500 μm (blue) and 0.700 μm (green) images with either of the longer wavelength images (red). These reveal that the lower half of the Juno image shows lower reflectance at 0.934 μm (Fig. 2B) than at 0.833 μm (Fig. 2A).

Fig. 3 shows the false color multispectral images of eight rotational phases of Juno. At rotation phases from ~0 to ~65° the images are generally round indicating that the intensities of the images at the four different wavelengths are quite similar in shape. However, at rotational phases of ~100 to ~165°, there is a consistent "bite" out of the lower right quadrant of each image. The lower part of these images is blue or blue-green in tint, indicating that the "red" image (0.833 or 0.934 μm) has a consistently lower relative intensity at these orientations. The same effect is seen whether the 0.833 or the 0.934 μm image is used in the false color image. At these rotational aspects, the reflectance of the lower portion of all images and especially in the lower right quadrant of the image is reduced at both wavelengths.

The locations of the central wavelengths for the four filters used in the present study are shown in Fig. 4. The

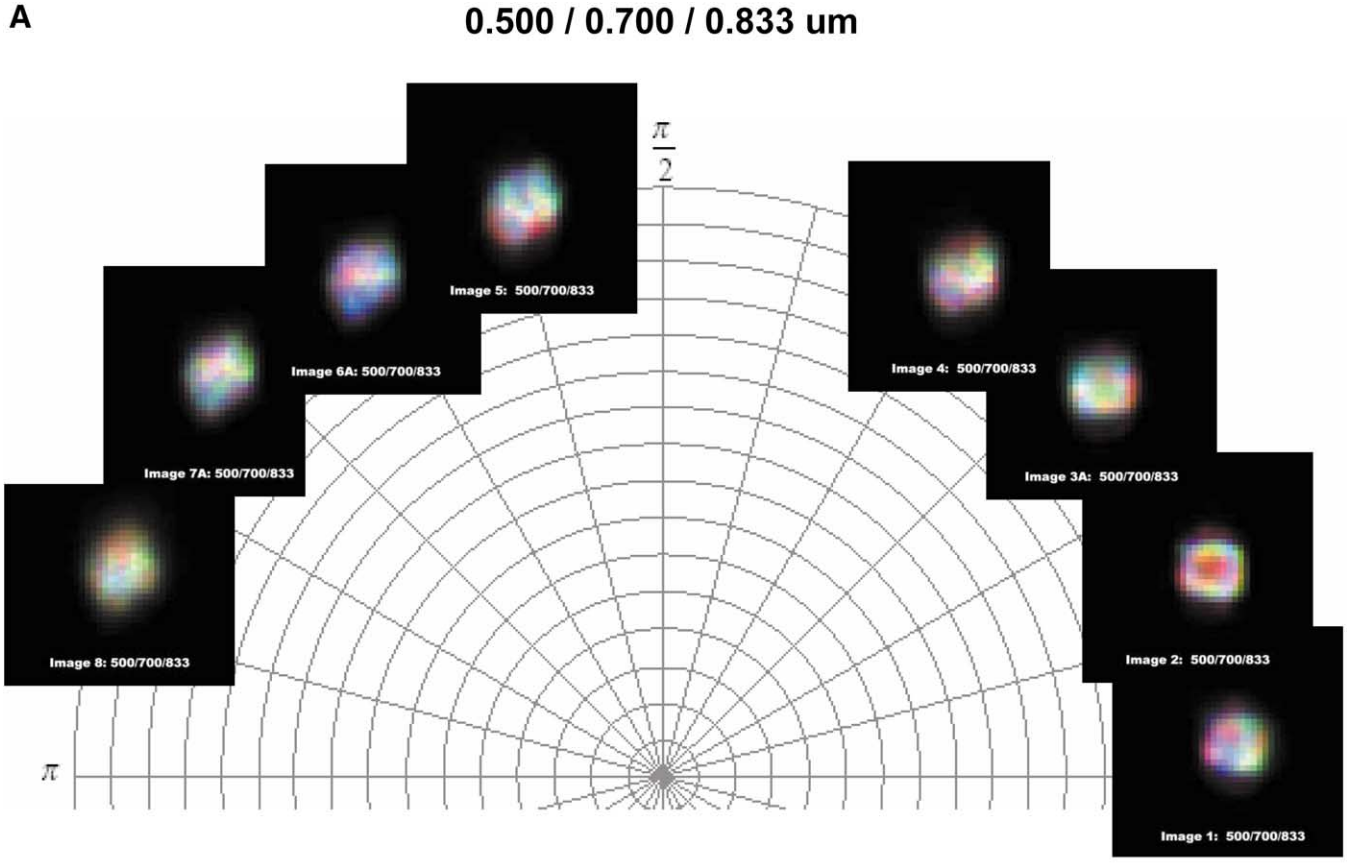
A
0.500 / 0.700 / 0.833 um
π/2
π
Image 5: 500/700/833
Image 6A: 500/700/833
Image 7A: 500/700/833
Image 8: 500/700/833
Image 4: 500/700/833
Image 3A: 500/700/833
Image 2: 500/700/833
Image 1: 500/700/833

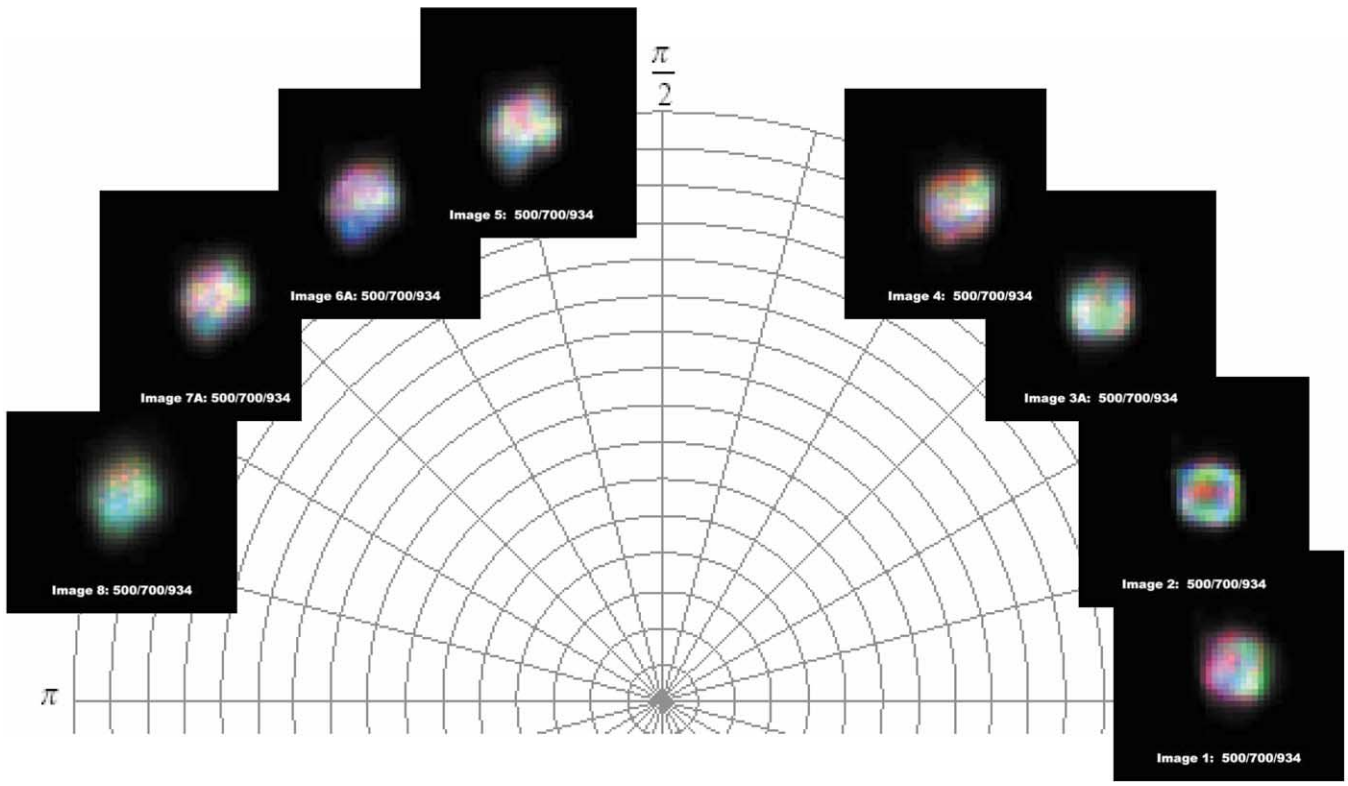
B
0.500 / 0.700 / 0.934 um
π/2
π
Image 5: 500/700/934
Image 6A: 500/700/934
Image 7A: 500/700/934
Image 8: 500/700/934
Image 4: 500/700/934
Image 3A: 500/700/934
Image 2: 500/700/934
Image 1: 500/700/934

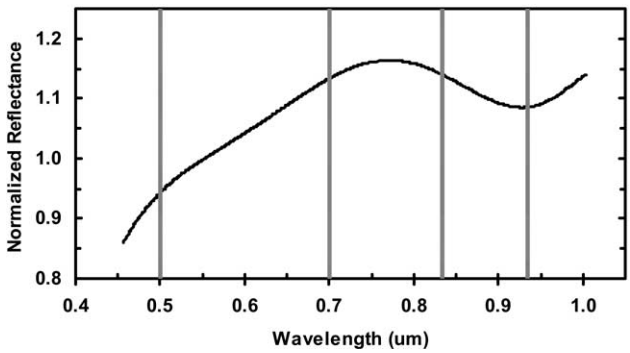

Fig. 4. The locations of the center wavelengths of the four filters used in the present study plotted over a spectral reflectance curve for 3 Juno. This spectral curve is a 12th order polynomial fit to the Juno CCD spectrum from the SMASS survey (Xu et al., 1995). The fitting was done to remove the effects of incompletely corrected atmospheric absorption features that were present in the original data.

relevant mineralogical feature is the broad absorption band located longward of ~0.8 μm and centered near 0.93 μm. This feature is due to the iron-bearing silicate minerals olivine and pyroxene. The 0.500 and 0.700 μm filters lie on the spectral continuum shortward of the mineral feature. The 0.833 and 0.934 μm filters are located on the short wavelength wing and near the center of the mineral absorption feature.

Interpretation of spectral variations on Juno

The relatively low 0.934 μm brightness in the lower portion of the Juno image (Fig. 1) can be interpreted as a result of the strengthening of the combined 1 μm olivine–pyroxene bands in the reflectance spectrum of this region relative to the rest of the surface. This stronger ~1 μm absorption feature, the effect of which is also seen in Fig. 2b, could be due to either an increase in the total abundance of olivine and pyroxene on the lower portion of the Juno image or a coarsening in the mean particle size of the surface material in this region. A substantial increase in total olivine and pyroxene abundance in this area is possible, but unlikely. S(IV)-type asteroids such as Juno have an average surface assemblage consisting predominantly (probably ≥80%) of olivine and pyroxene phases (Gaffey et al., 1993b). It would be very difficult to substantially increase the absorption band intensity by increasing the total abundance of these two mineral species. It is possible that metal actually comprises a major surface component on Juno, and that the lower region in the images is enriched in the silicate component relative to the average surface producing a stronger 1 μm silicate feature. However, the composition derived from previous analysis of the Juno spectrum (Gaffey et al., 1993b) suggests that metal is not a major component.

For typical planetary regolith materials, the relative intensity (feature strength relative to the background continuum, also termed contrast) of an absorption feature is maximized at the particular mean particle size which produces the maximum difference between the amount of light reflected at wavelengths outside the feature and the amount of light reflected at wavelengths near the center of the feature (Pieters, 1983). Lunar and asteroid regolith processes tend to produce particle sizes smaller than the optimum size for maximum relative absorption-feature intensity with olivine and pyroxene assemblages.

Meteorite parent bodies initially consisted of loose aggregates of fine-grained material accreted from the solar nebula. When such material was subjected to elevated temperatures (>400°C) for extended periods, larger grains grew at the expense of smaller grains by a series of processes collectively termed metamorphism. Increased temperatures accelerate this process, and the higher metamorphic grades of chondritic meteorites (e.g., types 5 and 6) are well-crystallized, coarse-grained materials. It is generally considered that in the chondrite parent bodies increasing depth corresponded to higher degrees of metamorphism (Haack et al., 1996).

Coarse-grained assemblages can also result from the slow cooling of molten rock at depth. Thus, in general, the deeper one goes into an intact asteroid that has experienced any significant degree of heating, the coarser the grain size of the assemblage. Therefore, a relatively coarse-grained region on Juno could be the result of excavation and exposure of a deeper internal layer by a large cratering event.

The lunar surface (as well as most other solid surfaces of airless bodies) exhibits a number of *bright craters.* These stand out against the darker lunar surface due to their relatively young age. More significantly, these bright craters exhibit strong absorption features. The cratering process has excavated relative coarse-grained bedrock material and spread it around the impact site. With increasing age, the brightness and strong absorption features of these craters decrease until they blend undetectably into the background (Pieters, 1977).

Thus, if an asteroid surface suffers no major impacts, the gardening process will eventually produce a fine-grained surface layer. Such an old surface will have relatively weak olivine and pyroxene absorption features because of the short optical path length of photons through the grains in the surface layer. A bedrock-excavating impact onto such a

Fig. 3. False color multispectral images (0.500/0.700/0.833 μm and 0.500/0.700/0.934 μm) of eight rotational phase of Juno. Relative rotational phasing is shown by the polar coordinate grid on which the images are plotted.

surface will produce a rejuvenated region with a fresh, coarser-grained surface layer exhibiting a stronger 1 μm absorption feature.

The multicolor spectral images of Juno suggest that a large ($\geq$100 km diameter), relatively young impact structure or a fresh ejecta layer for a smaller impact structure is located in the region corresponding to the lower quadrant of the images. It is possible, but not likely, that the background surface of Juno is the ancient original surface of the asteroid, covered with a fine-grained low metamorphic grade crust or (even less likely based on the S(IV) classification of Juno) by eruptive igneous rocks. It is more likely that the background surface is a mature asteroid regolith generated by a very long period of micrometeorite gardening.

Previous studies provide additional supporting evidence for the presence of a large color/albedo "spot" on the surface of Juno. Observations by Gaffey (in Degewij et al. 1978) showed a variation in the intensity of the 1 μm silicate absorption feature with rotation. Schroll et al. (1981) showed evidence of rotational color variations at visible wavelengths. Based on Fourier analysis of the lightcurve of Juno, Harris (1987) concluded that the lightcurve variation at visible wavelengths is primarily due to albedo variations across the surface of the asteroid. Each of these three independent results is consistent with the presence of the postulated large, relatively fresh impact crater on Juno.

It is difficult to evaluate the potential role of space weathering on the surface of Juno and its implications for the data presented here. Space weathering on asteroid surfaces is controlled by a number of factors (Ueda et al., 2002). The Galileo flyby of 243 Ida and the NEAR rendezvous with 433 Eros have indicated that the surface alteration differs between the two asteroids and both differ from the moon (Chapman, 1996). On the moon, increased weathering produces weakened absorption features, lowered albedos, and significant color changes (Pieters et al., 2000; Taylor et al., 2001). For Ida, there are significant color variations but virtually no albedo variations. Eros exhibits the opposite pattern, with virtually no color variations and large albedo variations (McFadden et al., 2001). Thus, the type of weathering process can clearly vary between otherwise grossly similar bodies (i.e., Eros and Ida are both S-type asteroids). Juno is also an S-type body, so at the moment we have no good model for space weathering effects expected.

Conclusions

Multispectral analyses of main belt asteroid 3 Juno taken at visible and near-infrared wavelengths with the 100-in. telescope at Mount Wilson reveal a region of apparent relatively low 0.934 μm brightness on the asteroid. This reduced near-Ir brightness may be interpreted as a strengthening of the combined 1 μm olivine–pyroxene bands in the reflectance spectrum of this region relative to the rest of the surface. If this is the case, then the feature may be a large ($\geq$100 km diameter) impact crater or a fresh ejecta blanket from a relatively young impact.

Acknowledgments

This research was made possible by a collaborative agreement between the Carnegie Institution of Washington and the Mount Wilson Institute. We are pleased to acknowledge support from the following individuals and foundations: Paul Gerstley, The Ahmanson Foundation, The Fred and Valerie Briggs Fellowship Fund, The Fletcher Jones Foundation, Stanley Zax and The Max Kampelman Fellowship Fund, and The Parsons Foundation.

References

Bell, J.F., Davis, D.R., Hartmann, W.K., Gaffey, M.J., 1989. Asteroids: The big picture, in: Binzel, R.P., Gehrels, T., Matthews, M.S. (Eds.), Asteroids II, Univ. of Arizona Press, Tucson, pp. 921–945.

Chapman, C.R., 1996. S-type asteroids, ordinary chondrites, and space weathering: the evidence from Galileo's fly-bys of Gaspra and Ida. Meteoritics Planet. Sci. 31, 699–725.

Degewij, J., Tedesco, E.F., Zellner, B., 1979. Albedo and color contrasts on asteroid surfaces. Icarus 40, 364–374.

Gaffey, M.J., Bell, J.F., Brown, R.H., Burbine, T.H., Piatek, J.L., Reed, K.L., Chaky, D.A., 1993a. Mineralogic variations within the S-type asteroid class. Icarus 106, 573–602.

Gaffey, M.J., Burbine, T.H., Binzel, R.P., 1993b. Asteroid spectroscopy and the meteorite connection: progress and perspectives. Meteoritics Planet. Sci. 28, 161–187.

Haack, H., Farinella, P., Scott, E.R.D., Keil, K., 1996. Meteoritic, asteroidal, and theoretical constraints on the 500 Ma disruption of the L chondrite parent body. Icarus 119, 182–191.

Harris, A.W., 1987. Fourier analysis of asteroid lightcurves: some preliminary results. Proc. Lunar Planet. Sci. Conf. 18, 385–386.

McFadden, L.A., Wellnitz, D.D., Schnaubelt, M., Gaffey, M.J., Bell III, J.F., Izenberg, N., Murchie, S., Chapman, C.R., 2001. Mineralogical interpretation of reflectance spectra of Eros from NEAR near-infrared spectrometer low phase flyby. Meteoritics Planet. Sci. 36, 1711–1726.

Millis, R.L., Wasserman, L.H., Bowell, E., Franz, O.G., White, N.M., Lockwood, G.W., Nye, R., Bertram, R., Klemola, A., Dunham, E., Baron, R.L., Elliot, J.L., Harris, A., Young, J.W., Faulkner, J., Stanton, R., Reitsema, H.J., Hubbard, W.B., Zellner, B., Lebofsky, L., Cruikshank, D.P., Macknik, L.S., Becklin, E.E., Morrison, D., Lonsdale, C.J., Kunkle, T.D., Lee, T., Gatley, I., A'Hearn, M.F., DuPoy, D.L., Nolthenius, R., Ford, H., McKenna, D., Placova, Z., Horne, K., Sandmann, W.H., Taylor, G.E., Tucker, R., 1981. The diameter of Juno from its occultation of AG + 0°1022. Astron. J 86, 306–313.

Pieters, C.M., 1977. Characterization of lunar mare basalt types-II: spectral classification of fresh mare craters. Proc. Lunar Sci. Conf. 8, 1037–1048.

Pieters, C.M., 1983. Strength of mineral absorption features in the transmitted component of near-infrared reflected light: first results from RELAB. J. Geophys. Res. 88, 9534–9544.

Pieters, C.M., Taylor, L.A., Noble, S.K., Keller, L.P., Watson, B., Morris, R.V., Allen, C.C., McKay, D.S., Wentworth, S., 2000. Space weath-

ering on airless bodies: resolving a mystery with lunar samples. Meteoritics Planet. Sci. 35, 1101–1107.

Schroll, A., Schober, H.J., Lagerkvist, C-I., 1981. Evidence for color variations on the surface of 3 Juno: new photoelectric UBV-observations. Astron. Astrophys. 104, 296–299.

Shelton, J.C., Schneider, T.G., McKenna, D., Baliunas, S.L., 1996. Results from Cassegrain adaptive optics system of the Mount Wilson 100-inch telescope. OSA Tech. Digest. 13, 43.

Shelton, J.C., Schneider, T.G., Baliunas, S.L., 1997. Science with the ADOPT system on Mount Wilson. Proc. SPIE 3126, 321.

Taylor, L.A., Pieters, C.M., Keller, L.P., Morris, R.V., McKay, D.S., Patchen, A., Wentworth, S., 2001. The effects of space weathering on Apollo 17 mare soils: petrographic and chemical characterization. Meteoritics Planet. Sci. 36, 285–299.

Ueda, Y., Hiroi, T., Pieters, C.M., Miyamoto, M., 2002. Changes of Band I center and BandII/I area ratio in reflectance spectra of olivine-pyroxene mixtures due to the space weathering and grain size effects. Proc. Lunar Planet. Sci. Conf. 33, (#2023).

Xu, S., Binzel, R.P., Burbine, T.H., Bus, S.J., 1995. Small main-belt asteroid spectroscopic survey: initial results. Icarus 115, 1–35.